Fuel 321 (2022) 124075

Contents lists available at ScienceDirect

Fuel

journal homepage: www.elsevier.com/locate/fuel

Full Length Article

# Improving $CO_2$ methanation performance by distributed feeding in a Ni-Mn catalyst fixed bed reactor

P. Aragüés-Aldea, A. Sanz-Martínez, P. Durán, E. Francés, J.A. Peña, J. Herguido *

*Catalysis Molecular Separations and Reactor Engineering Group (CREG), Aragon Institute of Engineering Research (I3A), Universidad Zaragoza, 50018 Zaragoza, Spain*

ARTICLE INFO

*Keywords:*
Methanation
Power to gas
Distributed feeding
Improved selectivity
Temperature profile

ABSTRACT

It has been successfully demonstrated the effect of feeding reactants in distributed manner for the reaction of methanation of $CO_2$. This operation mode has improved not only the selectivity towards $CH_4$, but also the overall process performance. A fixed bed reactor, loaded with Ni-Mn based catalyst, was operated co-feeding both $CO_2$ and $H_2$, but alternatively feeding one of them through several lateral inlets. Preserving the same global $W/F_{CO2}$ ratio, the side distribution of $CO_2$ allowed to clearly increase the activity of the process (e.g., at 375 °C, the conversion with distributed feeding was around 35% higher than that for the conventional one: $X_{CO2} = 0.12$ vs. $X_{CO2} = 0.09$). Furthermore, a substantially lower selectivity towards non-desired CO was obtained at any conversion level (e.g., $S_{CO} = 0.45$ vs. $S_{CO} = 0.70$, when $X_{CO2} = 0.10$). In addition, a more homogeneous temperature profile could be achieved in the bed without increasing the severity of hot spots appearance. On the contrary, side distribution of $H_2$ always led to similar or worse results than for the conventional co-feeding configuration.

## 1. Introduction

Along the last decades of continuous increase of greenhouse gas emissions and progressive depletion of fossil fuels, electricity of renewable origin (i.e., wind or sun) is making its way into the replacement of fossil fuels. However, there are still important drawbacks to overcome, like those derived from its intermittence and challenging storage. Additionally, the integration of different renewable energy sources, that induces a complex balance for supplying electricity to the power grid, has become a relevant task in many regions in the world, such as Europe [1,2].

An option for providing flexibility in this context is the *power to gas* strategy (P2G). According to this set of technologies, temporary surplus electricity could be used to produce hydrogen by electrolysis. On this way, renewable hydrogen and carbon dioxide, also with renewable origin (e.g., from biogas), could be converted into methane, which could be injected into any natural gas infrastructure, including the existing natural gas network present across the whole territory, as is the case of Europe [3]. According to Bailera et al. [4], a large number of researchers have revisited P2G technology in the last decade with energy storage purposes to better integrate renewable sources in the system. Accordingly, a remarkable increase in ongoing projects dealing with these processes have started along this period.

The reaction network for the carbon dioxide methanation process could be described through (r.1) to (r.4) reactions:

$$CO_2 + 4H_2 \rightleftharpoons CH_4 + 2H_2O; \quad \Delta H_r^0 = -165.1 kJ/mol \tag{r.1}$$

$$CO_2 + H_2 \rightleftharpoons CO + H_2O; \quad \Delta H_r^0 = +41.2 kJ/mol \tag{r.2}$$

$$CO + 3H_2 \rightleftharpoons CH_4 + H_2O; \quad \Delta H_r^0 = -206.3 kJ/mol \tag{r.3}$$

$$2CO \rightleftharpoons C_{(s)} + CO_2; \quad \Delta H_r^0 = -172.5 kJ/mol \tag{r.4}$$

To carry out (r.1) (*Sabatier* reaction) at an appreciable rate, a catalyst must be present. As described in literature, most of them are based in one or more supported metals [5]. Particularly, nickel is the most widely investigated one due to its low cost and availability while providing a good catalytic activity [6–15]. Cobalt exhibits similar selectivity than that of nickel but at a higher cost, what makes it less interesting [16,17]. Iron does not present much selectivity towards methane [18], however its combination with Ni improves the results in terms of selectivity and yield to $CH_4$ in the temperature range 250–350 °C [19]. Ruthenium has been highlighted as more active than nickel for $CO_2$ methanation, but as drawback, it is also substantially more expensive [20–23]. The same applies for Rhodium [24]. Catalyst support is the other essential element to be present. It can be the key to provide high surface area and enough

* Corresponding author.
*E-mail address:* jhergui@unizar.es (J. Herguido).

https://doi.org/10.1016/j.fuel.2022.124075
Received 12 November 2021; Received in revised form 16 March 2022; Accepted 31 March 2022
Available online 8 April 2022

dispersion of the active sites of the catalytic species, as well as mechanical and thermal resistance. Alumina ($Al_2O_3$), silica ($SiO_2$), titania ($TiO_2$), zirconia ($ZrO_2$) and niobite ($Nb_2O_5$) are among the most widely used supports [25], alumina being the most frequent.

Additionally, the promoters can help to improve the performance of methanation catalysts by enhancing the activation of $CO_2$ and $H_2$. Even though Ni-Mn catalysts were proposed a century ago as *Fischer-Tropsch* catalysts [26], it is only recently when Mn has received attention as a promoter for CO and $CO_2$ methanation. In fact, there are new studies [10,27,28] evidencing the high performance of Ni based catalyst where a cheap and abundant metal like Mn is used as support. However, some recent studies [29] show that using supported methanation catalysts with a high Mn/Ni ratio opens some room for side reactions (mainly the reverse *Water Gas Shift* reaction, r.2) to take place. On this way, a significantly higher selectivity to CO is obtained when high Mn proportions are included in the formulation of the methanation catalyst. Furthermore, Ni-$MnO_x$ supported on biomorphic carbon derived from lignocellulosic biomass residues, have recently been used as catalysts for this process [30], also presenting higher selectivities to CO at a given $CO_2$ conversion than those of their counterparts without Mn. Based on this fact, and in order to gain accuracy in determining the selectivity to undesired CO product, this type of catalysts has been considered useful and will be adopted in this work for the experimental study.

Regarding methanation technologies, a detailed review of P2G initiatives in which $CO_2$ methanation is carried out throughout catalytic processes [4], reveals that the most promising alternatives are based in fixed bed configurations. However, hot spots can appear in these cases due to the high exothermicity of the *Sabatier* reaction (r.1). This fact could favour CO and coke production, as well as catalyst deactivation by sintering [31,32], contributing to irreversible damages in the catalyst and by-products formation that could ruin the pursued objective of stability and high selectivity towards methane.

Despite the intense research effort devoted to optimize catalysts for methanation, there is still plenty room for improvement in selectivity and stability of this process through the application of reactor engineering strategies. To minimize hot spots, several reactor configurations are being under study in our lab as suitable substitutes of the traditional fixed bed reactor. Among them, fluidized bed reactors (FLBR) ensure a uniform temperature profile [19]. According to thermodynamic equilibria, temperatures above 400 °C will favor the generation of CO as a by-product (by reverse *Water Gas Shift* reaction -rWGS-, r.2), which could compete with $CO_2$ and react with $H_2$ (reverse *Methane Steam Reforming*, r.3 -rMSR-). CO generation might also promote deactivation of the catalyst by coking (by *Boudouard* reaction, r.4). With the aim of minimizing these adverse effects, two alternative reactor configurations have been studied: conventional fixed bed reactor and polytropic (i.e., distributed feed) fixed bed reactor. The parameters selected for comparison purposes have been the temperature profiles along the bed and performance in terms of $CO_2$ conversion, selectivity to $CH_4$ and stability of the process.

*Sabatier* reaction (r.1) could be considered as a series–parallel combination of both (r.2) and (r.3) hydrogenation reactions, where there is a successive attack of a compound ($CO_2$) by a reactive material ($H_2$) [33]. According with reactor engineering theory, contact type greatly influences the distribution of products. No matter what kind of reactor system is selected, when the fractional conversion of $CO_2$ is low, the fractional yield of the intermediate product CO is high. Nevertheless, CO selectivity would be higher when $CO_2$ stream is fed in a plug-flow mode and $H_2$ in a mixed flow mode.

The purpose of this research piece is to experimentally analyze the effect of different feeding configurations of the reactor, with the aim of maximizing selectivities towards $CH_4$ (i.e., minimize selectivities to CO), and optimistically also $CH_4$ yields, as well as trying to avoid thermal gradients generated by the exothermicity of the methanation process along the reactor. The concept of the polytropic-feed reactor (i.e., a fixed bed reactor with several side gas inlets), has already been used in our research group several decades ago in the lean distribution of oxygen in methane oxidative coupling reaction for maintaining a low partial pressure of oxygen along the bed minimizing combustion of methane [34], and in the regeneration of coked catalysts [35], thus reducing hot spots and the consequent sintering of the catalyst.

## 2. Experimental

### 2.1. Catalyst

Catalyst was nominally prepared as 5 $\%^{wt}$ Ni over manganese (III) oxide. It was produced by co-precipitation of both Ni and Mn nitrates using urea. The method was adapted from the one of Wei et al. [36]. Suitable proportions of the salts, urea, and distilled water [2.61 g of Ni $(NO_3)_2$, 35.4 g of $Mn(NO_3)_2$, 16.0 g of urea, and 150 mL of $H_2O$] were vigorously mixed at 80 °C for 3 h until completely dissolved; then, the solution was sonicated for 30 min. The solid obtained was dried overnight at 100 °C, and later on calcined at 600 °C for 3 h, using a heating ramp of 3 °C/min. Finally, it was crushed and sieved to a particle diameter between 100 and 160 μm. To demonstrate its correct preparation, it was subjected to a routine set of characterization techniques including XRD, BET, XRF and SEM.

### 2.2. Reaction setup

The solid bed was constituted by 0.25 g of catalyst 5$\%^{wt}$ Ni-$MnO_x$ diluted in 10.25 g of $Al_2O_3$ (SASOL Puralox SCCa-150/200) (inert) by mechanical mixture, resulting in a 12 cm high packed bed supported by a porous plate made in quartz (pore size minor or equal to 90 μm). Prior to methanation, the catalyst was activated at 500 °C and atmospheric pressure using hydrogen (0.5 bar) diluted in inert gas (Ar), with the aim of obtaining more reduced nickel species, considered as the active sites for the reaction.

Reactants were fed at 1 bar by means of mass flow controllers (*Alicat Scientific*) using always the stoichiometric molar ratio (r.1) $H_2$:$CO_2$ = 4:1. Reactive gases constituted 90 $\%^{v}$ of the total flow (0.9 bar), with Ar (0.05 bar) being used as inert and $N_2$ (0.05 bar) as internal standard. Total gas flow rate was always 250 STP mL·min$^{-1}$ for which negligible external and internal diffusional constraints were verified by previous methanation experiments with different catalyst particle sizes and feeding flow rates.

The experiments were carried out in a fixed bed vertical reactor made of quartz (inner diameter 1.3 cm) with three equidistant side feeding points located along the axial dimension of the bed (accounting from the distribution plate up at 3 cm, 6 cm, and 9 cm - $h_3$: $h_6$: $h_9$ -) and an upper (main) feed (at 12 cm - $h_{12}$ -). Also at these points, up to 5 thermocouples (1, 3, 6, 9 and 12 cm from the support quartz plate) were located. Fig. 1 shows a sketch of the several inlets and outlet of the reactor, as well as the thermocouple arrangement.

In the conventional configuration, both reactants $H_2$ and $CO_2$, were fully fed from the top of the bed, as it is usually done in the works described in literature. However, in the configurations with distributed feeding, hereafter referred to as 'polytropic' ones, one reactant ($H_2$ or $CO_2$), was always fed only through the main (upper) feed, while the second one was distributed homogeneously (i.e., with equal flow rates) or heterogeneously (i.e., with different flow rates) through the side inlets. This work only presents the results obtained for homogeneous distribution experiments. In them, each feed consisted in one fourth of the total flow, as it is presented in Fig. 1, for both 'Poly-$H_2$′' and 'Poly-$CO_2$′' configurations. The statistical significance of the differences between the experimental results of each feeding configuration was verified by experiments replication.

Heat was supplied by an electric oven. Temperature was measured by five "*K* type" thermocouples located along the bed inside a central quartz rod, with the purpose of analyzing temperature profiles in the bed. Thus, up to five temperatures ($T_{12}$, $T_9$, $T_6$, $T_3$ and $T_1$) were

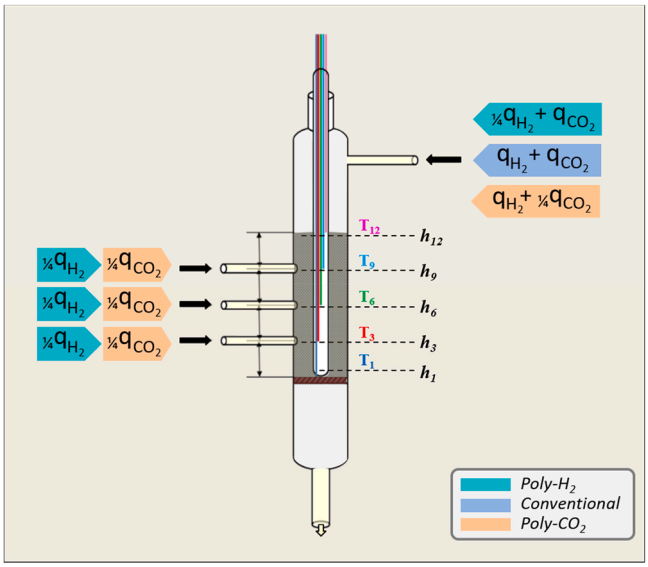


**Fig. 1.** Reactor sketch showing the position of thermocouples and the distribution of feed streams by configuration (*Conventional*, *Poly-$H_2$* and *Poly-$CO_2$*).

registered over time. In addition, the intermediate thermocouple ($T_6$) was used to control the oven power supply (controller *Eurotherm 3216*). Exhausted gases were analyzed by gas micro-chromatography (*Agilent 490 Micro GC*). The carbon balance closures of the experiments carried out always had values over 99.0%.

Several experimental series were always carried out, each one with a new batch of fresh catalyst. Typical series consisted of the following set of experiments:

- (i) a dynamic experiment using one of the three aforementioned feeding configurations and varying temperatures along the time on stream (TOS). Temperature was set from 400 to 250 °C (down step), in intervals of 25 °C (45 min TOS at each temperature, except 60 min at 400 °C for stabilization purposes),
- (ii) a long-lasting isothermal experiment (for 240 min at 400 °C) maintaining same configuration as in experiment (i), and
- (iii) and (iv) two isothermal experiments (60 min TOS at 400 °C) at the remaining two configurations.

The only difference between these series was the sequential order in which each experiment (*i*, *ii*, *iii*, and *iv)* was implemented. Prior to each experiment, catalyst was reduced using a gas stream of $H_2$ (0.5 bar) diluted in Ar (500 °C for 2 h) with the same total flow rate as that used in the reaction.

## 3. Results and discussion

### 3.1. Catalyst characterization

Surface area for fresh catalyst samples (i.e., before reaction), was 21.1 ± 0.1 $m^2/g$ according to BET measurements. Ni and Mn atomic metal contents obtained by XRF were 4.6%$^{wt}$ and 70.1%$^{wt}$ respectively for fresh catalysts, and 4.3%$^{wt}$ and 67.1%$^{wt}$ respectively for reduced catalysts before the reaction step. Apparently, both metals exhibited an oxidation state of + 2 (i.e., NiO and MnO species) after the reduction step under hydrogen atmosphere at 500 °C. Higher temperatures, around 700 °C, would have been required [28] to fully reduce the nickel oxide, so that metallic Ni and NiO could actually be coexisting in the activated catalysts.

Fig. 2a shows the obtained X-ray diffractograms for both fresh and activated catalysts. $Mn_2O_3$ is the only manganese phase observed for fresh catalysts, while it seems to be completely reduced to MnO in the activated sample. Peaks corresponding to nickel could not be observed in these XRD measurements, what is attributed to a small proportion, low crystallinity and/or small size of its structures on the catalyst surface. Finally, according to the SEM observation, the catalyst has a granular structure with an average grain size of around 1 μm. A representative photograph of the catalyst can be seen in Fig. 2b. Red and green points represent Mn and Ni EDX mapping values, respectively, showing dispersed Ni and Mn particles over the entire surface and letting appreciate the homogeneity of their distribution. Their quantification gives a Ni/(Ni + Mn) ratio of 0.057 %$^{wt}$, which matches with the nominal value.

### 3.2. Dynamic experiments (T-Dynamic). Methanation at different temperatures.

Fig. 3 shows both $CO_2$ and $H_2$ conversions for three series, each of them with different feeding configuration (conventional, $H_2$ distributed, and $CO_2$ distributed feeds). The average repeatability error in terms of reagent conversion results can be considered less than 5%. This value was estimated from the replica (not shown) of a series of 44 experimental data homogeneously distributed in the temperature range 250–400 °C. Conversion ($X_{CO2}$) has been defined in a traditional way as

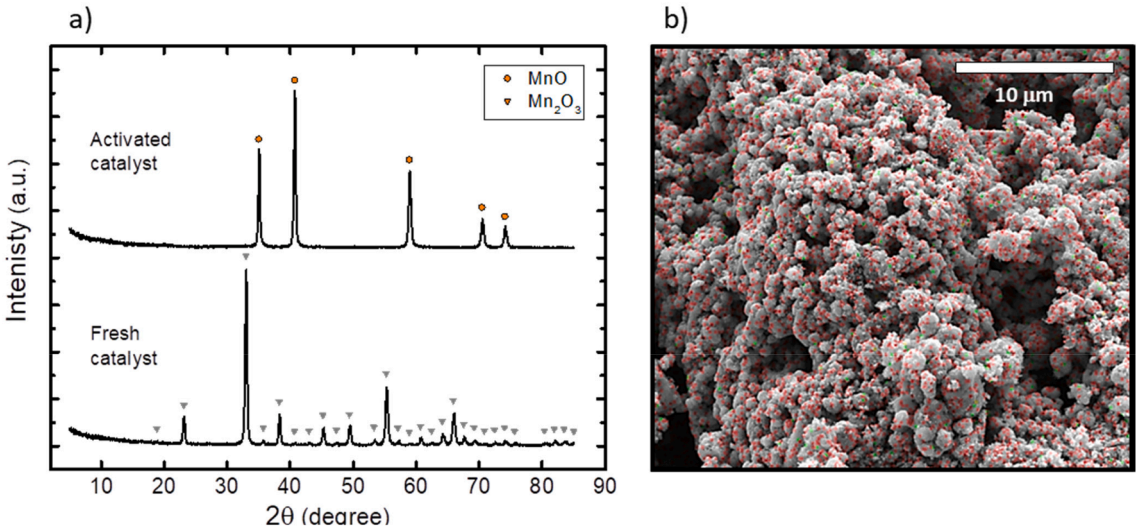


**Fig. 2.** XRD diffractograms for fresh and reduced catalyst (a), and a representative SEM-EDX photograph from a fresh catalyst sample (b).

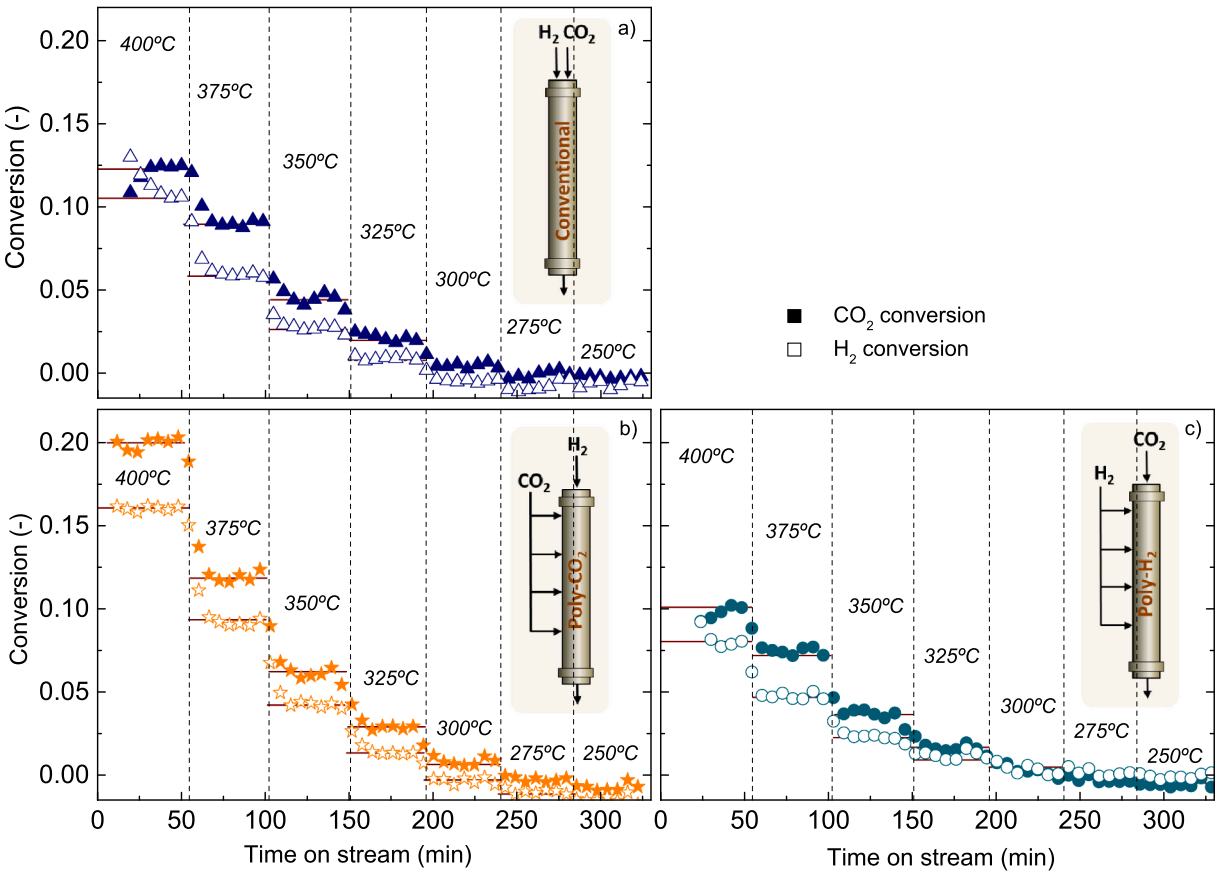


**Fig. 3.** Effect of temperature on conversion of reactants as a function of the feeding configuration in the fixed bed reactor. a) Conventional feeding, b) Side distribution of $CO_2$ (*Poly-CO₂*), and c) Side distribution of $H_2$ (*Poly-H₂*). Solid symbols: $CO_2$ conversion; hollow symbols: $H_2$ conversion. Horizontal lines only for visual guidance.

in (eq.1). Similarly, (eq.2) presents the way in which CO selectivity ($S_{CO}$) has been calculated throughout the text.

$$X_{CO2} = \frac{f^{in}_{CO_2} - f^{out}_{CO_2}}{f^{in}_{CO_2}} \quad (1)$$

$$S_{CO} = \frac{f^{out}_{CO}}{f^{out}_{CH_4} + f^{out}_{CO}} \quad (2)$$

where $f^j_k$ denotes the molar flow of "$k$" species entering ($j = in$) or leaving ($j = out$) the reactor.

## 4. Stability

Even though there is a previous reduction of the catalyst, and a certain period of stabilization of its oxidation state might be necessary, the values of conversion reveal a nearly stable behavior throughout the time-on-stream at 400 °C. This is especially true when lateral side feeding of carbon dioxide is used (i.e., 'Poly-$CO_2$' configuration). Moreover, for the rest of temperatures subsequently adopted in the bed, there is a clear stable fashion along their respective 45 min periods. This behavior was seen along the experiments without any deactivation indication.

## 5. Selectivity

Despite a stoichiometric $H_2$:$CO_2$ molar ratio of 4:1 being always fed to the reactor, $CO_2$ presents conversion values above those offered by $H_2$ even for low temperatures. This points out that *Sabatier* reaction (r. 1) characterized by the adopted 4:1 ratio is not the only reaction present. Reverse WGS (r.2) with a 1:1 M ratio could help to accommodate these results. Thus, the higher the contribution of rWGS to the global process, the lower is the hydrogen conversion with respect to the one of carbon dioxide and, consequently, the higher the selectivity to carbon monoxide in the exhaust gases. No other gaseous by-products apart from CO were detected under the conditions tested. Detection limit for CO in μGC is in the range of 50 ppm.

## 6. Activity

Regarding the level of activity exposed by the system, actual conversions were always far away from the predicted equilibrium. Equilibrium conversions were never achieved, not even at the highest temperature tested (400 °C). This can be attributed to the relatively short range of reactor space-times used in this work, implying that the reaction process is under kinetic control. Therefore, as it could be expected, an increase in the reaction temperature results in greater kinetics and consequently in higher conversions.

Nevertheless, it is worth mentioning that the experimental values of $CO_2$ and $H_2$ conversion are clearly higher when the reactor was operated under the 'Poly-$CO_2$' configuration (Fig. 3). Bearing in mind the distribution of gas streams in each feeding configuration (see Fig. 1), only when hydrogen is side distributed (Poly-$H_2$) it is expected a clear increase in the space–time value respecting the one foreseeable in the conventional configuration. The corresponding space–time value for 'Poly-$CO_2$' configuration must be only slightly higher than the one for conventional configuration. However, from Fig. 3, the results of conversion for conventional configuration at a given temperature (e.g., at 375 °C $X_{CO2}$ = 8.8 and $X_{H2}$ = 5.9) get worse when working with configuration 'Poly-$H_2$' (e.g., at 375 °C $X_{CO2}$ = 7.4 and $X_{H2}$ = 4.7) and

they are greatly improved when working with the 'Poly-$CO_2$' configuration (e.g., at 375 °C $X_{CO2} = 11.9$ and $X_{H2} = 9.2$). Therefore, the contact mode significantly influences the reaction process, allowing more reaction for that last arrangement.

Fig. 4 represents values of selectivity to carbon monoxide as a function of carbon dioxide conversion. In general, for sequential processes such as the hydrogenation described by reactions (r.2) and (r.3), it is important comparing *iso*-conversional selectivities with the aim to correctly discriminate the more selective way to work; otherwise, as a rule, the higher the conversion, the lower the selectivity towards intermediate products.

As it can be seen, for temperatures lower than around 325 °C, selectivities to CO are roughly 100% regardless which feeding configuration is used in the reactor. This agrees with very low $CO_2$ conversions and represents the worst scenario for the desired process of carbon dioxide methanation, giving very low reaction of carbon dioxide and no yield to methane. When higher $CO_2$ conversions are reached (in this case by increasing temperature for a given $W/F_{CO2}$ ratio), the selectivity to CO decreases as desired. This drop is especially significant for 'Poly-$CO_2$' configuration.

Although it would probably be necessary to carry out more experiments with higher $W/F_{CO2}$ ratios in order to verify this tendency for higher conversions (higher than $X_{CO2}$ of around 20%, which is the top value reached in experiments of the series shown in these figures), it can be concluded that for any conversion, the fixed bed reactor with a side distributed configuration of carbon dioxide is more selective towards methane. And, no matter what temperature is used, the methane yield will always be higher in 'Poly-$CO_2$' configuration than in the other two.

No great differences are seen among selectivity curves of 'Poly-$H_2$' and 'Conventional' configurations for low temperatures and conversions. However, when working at higher temperatures (375 and 400 °C) higher selectivities towards CO are found for 'Poly-$H_2$' configuration. This agrees with the hypothesis of considering side distribution of hydrogen as the less selective way of operation to produce methane. However, for both configurations at 400 °C there is an unusual drastic increase in the selectivity curve up to values close to 100%. This undesired behaviour is not appreciated for the 'Poly-$CO_2$' configuration.

There is not a clear reason for this last effect. It has been explained as an artifact having to do with the non-stationary state of the system, bearing in mind that those data at 400 °C conform the beginning of each experimental series with a new catalyst batch. In fact, as it will be exposed throughout the next section, there will be an important decrease in CO selectivity with TOS for both 'Poly-$H_2$' and 'Conventional' configuration working at 400 °C.

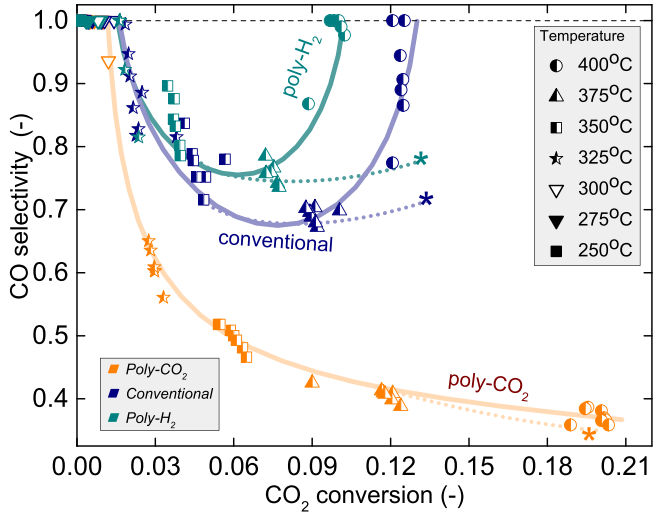


**Fig. 4.** Selectivity to CO vs. $CO_2$ conversion as a function of the feeding configuration in the fixed bed reactor and temperature set point. Curves only for visual guidance. Asterisk symbols (*) correspond to long-term values (TOS = 500 min) obtained for each feeding configuration.

### 6.1. *Isothermal experiments.*

Fig. 5 shows the evolution of both activity (expressed as $CO_2$ conversion) and selectivity (towards CO) with time (see (eq.1) and (eq.2)) in long-term isothermal experiments (400 °C) carried out subsequently to the *T-dynamic* ones. The TOS origin for these graphs is the time of beginning of *T-dynamic* runs, and the results obtained for the 400 °C period have been included in Fig. 5 before the time-break in the abscissa axis. The break time comprises the period of reaction stages at lower temperatures (375 to 250 °C).

Regarding activities, Fig. 5a, although the process is more stable in the final stage (TOS > 400 min) than at the beginning (TOS less than 50 min), a slight variation in the catalytic activity still persists for all feeding configurations. On the other hand, the higher activity achieved in the pseudo-stationary state with the $CO_2$ distributed configuration (Poly-$CO_2$) is clear, compared to the one for the other two configurations, which present similar conversion between them.

Instability, in terms of selectivity to CO, is even greater (see Fig. 5b), probably related to a still unfinished process of structural and/or superficial adjustment of the catalyst. Once again, a different behavior is observed for the configuration with distributed $CO_2$ feeding (clearly less selective to CO) compared to the other two.

Summarizing, long-lasting isothermal experiments at 400 °C and after a global TOS of 500 min still show some variation in activity and

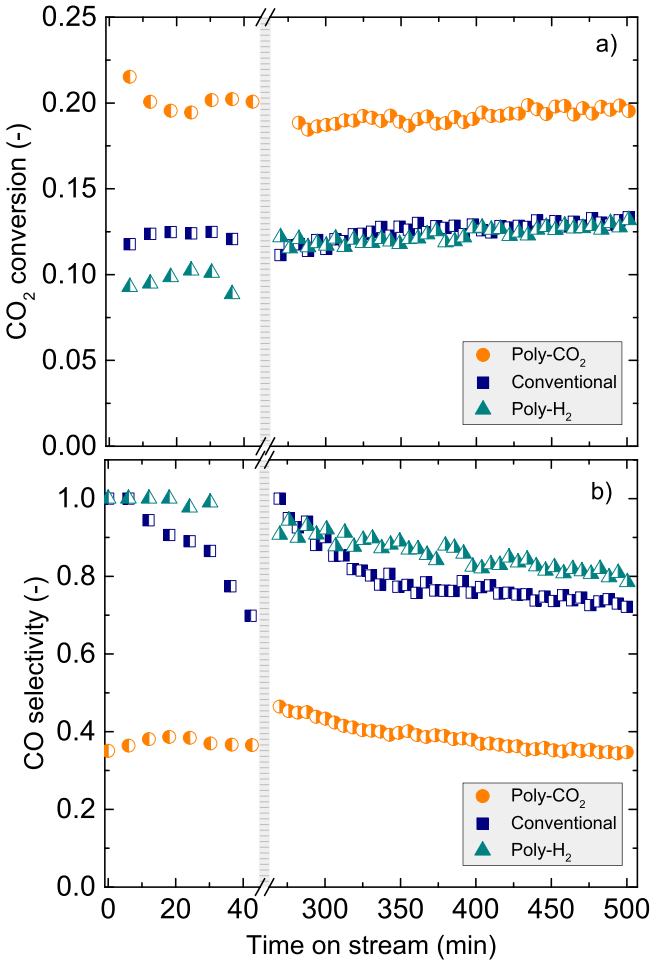


**Fig. 5.** Time evolution of (a) $CO_2$ conversion, and (b) selectivity to CO throughout isothermal steps working at 400 °C.

selectivity, albeit very slightly. Nevertheless, both tendencies have a positive sense for the process (i.e., there is a trend to increase activity and decrease selectivity to CO), and a nearly steady state can be envisaged for the catalyst at that time.

Finally, it is worth noting that the pairs of final values [$X_{CO2}$, $S_{CO}$] at TOS = 500 min, do not differ much from the initial ones at TOS = 0 min in the case of the 'Poly-$CO_2$′' configuration, but they do for the other two. These three values have been graphed using asterisk symbols in Fig. 4. Thus, it can be verified that $S_{CO}$ vs $X_{CO2}$ curves for the two configurations ('Poly-$H_2$′' and 'Conventional') also tend to decrease. Therefore, their U-shapes seen in Fig. 4 are confirmed to be only a consequence of the instability of the experimental values coming from the initial isothermal stages (400 °C) of *T-dynamic* experiments.

### 6.2. Temperature profiles along the bed

The study of reaction yields was complemented with an analysis of temperature profiles along the bed of solids. In previous studies [37,38] the effect of distributed feed to minimize thermal gradients in the bed was analyzed for both homogeneous and inhomogeneous side-flow distributions, using a 10%$^{wt}$ $Ni/Al_2O_3$ catalyst. In general, distributed feed reduced thermal gradients. Moreover, homogeneous flow distributions showed lower temperature gradients regardless of the reactant distributed ($CO_2$ or $H_2$). Additionally, for stoichiometric feed ratio ($H_2$: $CO_2$ = 4:1) slightly better conversions were obtained when $CO_2$ was distributed. In this work a homogeneous flow distribution (i.e., similar flow rate of the distributed gas through each inlet) was always used.

Temperature profiles (i.e., values from $T_1$ to $T_{12}$ according to Fig. 1) were measured and recorded in terms that enable their evolution over time to be viewed. At the beginning of each experimental series, coinciding with the moment when the reagents were introduced into the bed, an increase in temperature $\Delta T$ (actual temperature minus temperature set point) was always observed for each $h_i$, subscript "$i$" being the position in the packed bed (i.e., at 1, 3, 6, 9, and 12 cm above porous plate support). Moreover, this $\Delta T$ can be directly related to the appearance of hot spots in the packed bed and therefore to the possibility of thermal damage to the catalyst and its consequent deactivation. The greatest risk occurs when working in the high temperature range (i.e., $T_6$ = 400 °C). It is worth noting that height $h_6$ (6 cm above the distribution plate) represents the temperature imposed as set-point by the PID temperature controller.

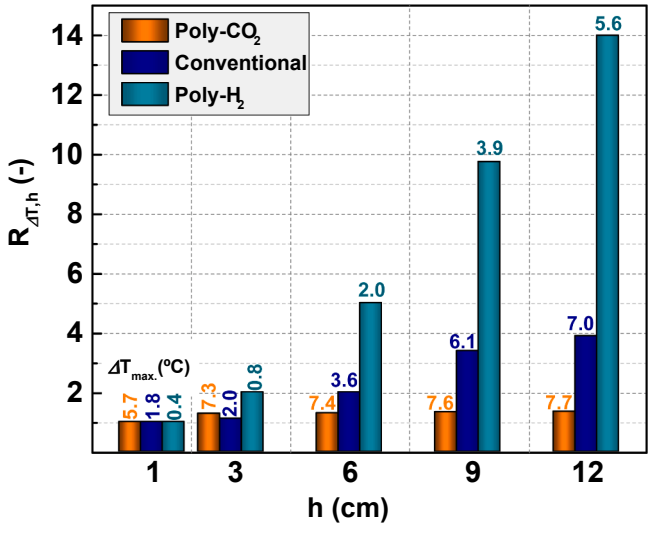


**Fig. 6.** Relative temperature increase profiles, $R_{\Delta T,h}$, in the packed bed for the three different feeding configurations. Set point $T_6$ = 400 °C. Bar value labels represent the maximum temperature increase ($\Delta T_{max}$) reached at each bed height ($h_i$).

Fig. 6 represents the bed profiles of relative temperature increase produced by the exothermic reaction process. To that end, the relative increase at each height $h$ ($R_{\Delta T,h}$) has been defined respecting to the one obtained at the bottom of the bed ($h$ = *1*) according to (eq. 3); $\Delta T_{max}$ being the maximum temperature increase value reached at each bed height.

$$R_{\Delta T,h} = \frac{(\Delta T_{max})_h}{(\Delta T_{max})_{h=1cm}} \quad (3)$$

As it can be seen, the $CO_2$ side distribution leads to a qualitatively different profile than the other two feeding options. In fact, a very homogeneous profile of $R_{\Delta T,h}$ is observed throughout the length of the bed for 'Poly-$CO_2$′' while for 'Conventional' and 'Poly-$H_2$′' configurations profiles are markedly pronounced, particularly in the latter case. It should be noted that specific $\Delta T_{max}$ values for 'Poly-$CO_2$′' are greater than for conventional mode, and these greater than those for 'Poly-$H_2$′'. That is, the same relative arrangement of values is observed as for the level of conversion achieved with each configuration (see Figs. 4 and 5).

Bearing in mind the objective of reaching high activity levels without promoting the appearance of hot spots along the bed, this study indicates that distributing the reactant $CO_2$ could be a good option. In fact, really higher conversions can be achieved for this 'Poly-$CO_2$′' configuration while maintaining a similar value of $\Delta T_{max}$ than the higher value found for the other two configurations (at $h_{12}$ for all of them), even with a much lower conversion. In any case, at the working conditions used in this study $\Delta T_{max}$ values are always lower than around 8 °C, which represents an acceptable value without high risk of sintering of the active phase of the catalyst or carbon deposition (r.4) on its surface.

## 7. Conclusions

The influence of side distributed feeding on the $CO_2$ methanation process (i.e., *Sabatier* reaction) is clearly verifiable when an *ad hoc* Ni-Mn based catalyst is used. Such a prone to CO production lab-made catalyst makes the study sensitive enough to assess the effect of reactor configuration on the process selectivity.

A significantly enhanced $CO_2$ methanation activity and selectivity is achievable by simply changing the reactor feeding configuration. Certainly, side distribution of $CO_2$ ('Poly-$CO_2$′' configuration) leads to an improvement of activity, providing a noteworthy conversion enhancement at all temperatures (e.g. at 375 °C, $X_{CO2}$ = 11.9 and $X_{H2}$ = 9.2) compared to both 'Conventional' ($X_{CO2}$ = 8.8 and $X_{H2}$ = 5.9) and 'Poly-$H_2$′' ($X_{CO2}$ = 7.4 and $X_{H2}$ = 4.7) configurations.

Likewise, for any conversion achieved, a 'Poly-$CO_2$′' arrangement always allows a lower selectivity to CO than the 'Conventional' one. In contrast, 'Poly-$H_2$′' configurations lead to higher selectivities to CO.

The effects on selectivity are consistent with a series–parallel reaction scheme in which $H_2$ acts as an attacking reagent on $CO_2$. Thus, the route of both rWGS and rMSR consecutive hydrogenation reactions (i.e., reverse *Water Gas Shift reaction* and subsequent reverse *Methane Steam Reforming*) dominates the process when a catalyst like the Ni-Mn one is used. These findings lead to conclude that, preserving the same global $W/F_{CO2}$ ratio and no matter what temperature is used, the methane yield will always be higher in 'Poly-$CO_2$′' configuration than in the other two.

Regarding longitudinal profiles in the bed, side distribution of $CO_2$ ('Poly-$CO_2$′' configuration) allows to obtain a more spread location of reaction along it. Thus, a more homogeneous $\Delta T$ profile is observed along the bed for 'Poly-$CO_2$′' feeding, while not exceeding $\Delta T_{max}$ values from the other configurations.

Consequently, acting on the feed configuration in a fixed bed reactor proves to be a tool to improve its performance and therefore an advantage to consider in the design/operation of any methanation reactor in the power to gas (P2G) strategy.

## Declaration of Competing Interest

The authors declare that they have no known competing financial interests or personal relationships that could have appeared to influence the work reported in this paper.

## Acknowledgements

Financial support for this work has been provided by the Spanish *Ministerio de Economía y Competitividad* (MINECO), through project CTQ2016-77277-R and *Ministerio de Ciencia e Innovación* (MICINN), through project PID2019-104866RB-I00. In addition, *Gobierno de Aragón* (Aragón, Spain) is gratefully acknowledged for the financial support (European Social Fund - FEDER) of the consolidated research *Catalysis, Molecular Separations and Reactor Engineering Group* (CREG) (T43_20R). Authors would like to acknowledge the use of *Servicio General de Apoyo a la Investigación-SAI* (Universidad de Zaragoza).

## References

[1] Parliament E. Directive 2009/28/EC of the European Parliament and of the Council of 23 April 2009 on the promotion of the use of energy from renewable sources and amending and subsequently repealing Directives 2001/77/EC and 2003/30/EC. Europe 2009.
[2] European Parliament. Directive (EU) 2018/2001 of the Euroepan Parliament and of the Councilof 11 December 2018 on the promotion of the use of energy from renewable sources (recast). 2018.
[3] van Leeuwen C, Mulder M. Power-to-gas in electricity markets dominated by renewables. Appl Energy 2018;232:258–72. https://doi.org/10.1016/j.apenergy.2018.09.217.
[4] Bailera M, Lisbona P, Romeo LM, Espatolero S. Power to Gas projects review: Lab, pilot and demo plants for storing renewable energy and $CO_2$. Renew Sustain Energy Rev 2017;69:292–312. https://doi.org/10.1016/j.rser.2016.11.130.
[5] Pandey D, Deo G. Effect of support on the catalytic activity of supported Ni–Fe catalysts for the $CO_2$ methanation reaction. J Ind Eng Chem 2016;33:99–107. https://doi.org/10.1016/j.jiec.2015.09.019.
[6] Ma S, Tan Y, Han Y. Methanation of syngas over coral reef-like Ni/$Al_2O_3$ catalysts. J Nat Gas Chem 2011;20(4):435–40. https://doi.org/10.1016/S1003-9953(10)60192-2.
[7] Tada S, Shimizu T, Kameyama H, Haneda T, Kikuchi R. Ni/CeO2 catalysts with high $CO_2$ methanation activity and high $CH_4$ selectivity at low temperatures. Int J Hydrogen Energy 2012;37(7):5527–31. https://doi.org/10.1016/j.ijhydene.2011.12.122.
[8] Garbarino G, Riani P, Magistri L, Busca G. A study of the methanation of carbon dioxide on Ni/$Al_2O_3$ catalysts at atmospheric pressure. Int J Hydrogen Energy 2014;39(22):11557–65. https://doi.org/10.1016/j.ijhydene.2014.05.111.
[9] Gao J, Liu Q, Gu F, Liu B, Zhong Z, Su F. Recent advances in methanation catalysts for the production of synthetic natural gas. RSC Adv 2015;5(29):22759–76. https://doi.org/10.1039/C4RA16114A.
[10] Zhao K, Li Z, Bian Li. $CO_2$ methanation and co-methanation of CO and $CO_2$ over Mn-promoted Ni/$Al_2O_3$ catalysts. Front Chem Sci Eng 2016;10(2):273–80. https://doi.org/10.1007/s11705-016-1563-5.
[11] Zhou R, Rui N, Fan Z, Liu C. Effect of the structure of Ni/$TiO_2$ catalyst on $CO_2$ methanation. Int J Hydrogen Energy 2016;41:22017–25. https://doi.org/https://doi.org/10.1016/j.ijhydene.2016.08.093.
[12] Le TA, Kim MS, Lee SH, Kim TW, Park ED. CO and $CO_2$ methanation over supported Ni catalysts. Catal Today 2017;293–294:89–96. https://doi.org/10.1016/j.cattod.2016.12.036.
[13] Miguel CV, Mendes A, Madeira LM. Intrinsic kinetics of $CO_2$ methanation over an industrial nickel-based catalyst. J CO2 Util 2018;25:128–36. https://doi.org/10.1016/J.JCOU.2018.03.011.
[14] Vogt C, Groeneveld E, Kamsma G, Nachtegaal M, Lu Li, Kiely CJ, et al. Unravelling structure sensitivity in $CO_2$ hydrogenation over nickel. Nat Catal 2018;1(2):127–34. https://doi.org/10.1038/s41929-017-0016-y.
[15] Zhang Lu, Gao Z, Bao L, Ma H. Influence of the supports $ZrO_2$ on selective methanation of CO over the nickel supported catalysts. Int J Hydrogen Energy 2018;43(19):9287–95. https://doi.org/10.1016/j.ijhydene.2018.03.185.
[16] Le TA, Kim MS, Lee SH, Park ED. CO and $CO_2$ Methanation Over Supported Cobalt Catalysts. Top Catal 2017;60(9-11):714–20. https://doi.org/10.1007/s11244-017-0788-y.
[17] Li W, Nie X, Jiang X, Zhang A, Ding F, Liu M, et al. ZrO2 support imparts superior activity and stability of Co catalysts for $CO_2$ methanation. Appl Catal B Environ 2018;220:397–408.
[18] Kirchner J, Anolleck JK, Lösch H, Kureti S. Methanation of $CO_2$ on iron based catalysts. Appl Catal B Environ 2018;223:47–59. https://doi.org/10.1016/J.APCATB.2017.06.025.
[19] Martínez-Visus I, Sanz-Martínez A, Francés E, Herguido J, Peña J. $CO_2$ methanation in fluidized bed reactor for production of synthetic natural gas (P2G process) with nickel-iron based catalyst. In: Ed. GD et al. – A, editor. 3th Int. Congr. ANQUE-ICCE- Student Conf. B. Abstr., Santander (Spain): 2019.
[20] Janke C, Duyar MS, Hoskins M, Farrauto R. Catalytic and adsorption studies for the hydrogenation of $CO_2$ to methane. Appl Catal B Environ 2014;152-153:184–91. https://doi.org/10.1016/j.apcatb.2014.01.016.
[21] Aziz MAA, Jalil AA, Triwahyono S, Ahmad A. $CO_2$ methanation over heterogeneous catalysts: recent progress and future prospects. Green Chem 2015;17(5):2647–63. https://doi.org/10.1039/C5GC00119F.
[22] Lazdans A, Dace E, Gusca J. Development of the Experimental Scheme for Methanation Process. Energy Procedia 2016;95:540–5. https://doi.org/10.1016/J.EGYPRO.2016.09.082.
[23] Bermejo-López A, Pereda-Ayo B, González-Marcos JA, González-Velasco JR. Mechanism of the $CO_2$ storage and in situ hydrogenation to $CH_4$. Temperature and adsorbent loading effects over Ru-CaO/$Al_2O_3$ and Ru-$Na_2CO_3$/$Al_2O_3$ catalysts. Appl Catal B Environ 2019;256:117845. https://doi.org/https://doi.org/10.1016/j.apcatb.2019.117845.
[24] Swalus C, Jacquemin M, Poleunis C, Bertrand P, Ruiz P. $CO_2$ methanation on Rh/γ-$Al_2O_3$ catalyst at low temperature: "In situ" supply of hydrogen by Ni/activated carbon catalyst. Appl Catal B Environ 2012;125:41–50. https://doi.org/https://doi.org/10.1016/j.apcatb.2012.05.019.
[25] Frontera P, Macario A, Ferraro M, Antonucci PierLuigi. Supported Catalysts for $CO_2$ Methanation: A Review. Catalysts 2017;7(12):59. https://doi.org/10.3390/catal7020059.
[26] Enger BC, Holmen A. Nickel and Fischer-Tropsch Synthesis Catal Rev 2012;54(4):437–88. https://doi.org/10.1080/01614940.2012.670088.
[27] Vrijburg WL, Moioli E, Chen W, Zhang M, Terlingen BJP, Zijlstra B, et al. Efficient Base-Metal NiMn/$TiO_2$ Catalyst for $CO_2$ Methanation. ACS Catal 2019;9(9):7823–39. https://doi.org/10.1021/acscatal.9b0196810.1021/acscatal.9b01968.s001.
[28] Vrijburg WL, Garbarino G, Chen W, Parastaev A, Longo A, Pidko EA, et al. Ni-Mn catalysts on silica-modified alumina for $CO_2$ methanation. J Catal 2020;382:358–71. https://doi.org/10.1016/j.jcat.2019.12.026.
[29] Pastor-Pérez L, Patel V, Le Saché E, Reina TR. $CO_2$ methanation in the presence of methane: Catalysts design and effect of methane concentration in the reaction mixture. J Energy Inst 2020;93(1):415–24. https://doi.org/10.1016/j.joei.2019.01.015.
[30] Merchán XJ. Development of $CO_2$ methanation catalysts from lignocellulosic residues. Zaragoza (Spain): Universidad de Zaragoza; 2019.
[31] Rönsch S, Schneider J, Matthischke S, Schlüter M, Götz M, Lefebvre J, et al. Review on methanation – From fundamentals to current projects. Fuel 2016;166:276–96. https://doi.org/10.1016/j.fuel.2015.10.111.
[32] Champon I, Bengaouer A, Chaise A, Thomas S, Roger AC. Modelling the sintering of nickel particles supported on γ-alumina under hydrothermal conditions. Catalysts 2020;10:1–11. https://doi.org/10.3390/catal10121477.
[33] Champon I, Bengaouer A, Chaise A, Thomas S, Roger AC. Carbon dioxide methanation kinetic model on a commercial Ni/$Al_2O_3$ catalyst. J CO2 Util 2019;34:256–65. https://doi.org/10.1016/j.jcou.2019.05.030.
[34] Santamaría J, Menéndez M, Peña JA, Barahona JI. Methane oxidative coupling in fixed bed catalytic reactors with a distributed oxygen feed. A simulation study. Catal Today 1992;13(2-3):353–60. https://doi.org/10.1016/0920-5861(92)80160-O.
[35] Finol C, Menéndez M, Santamaría J. Regeneration of Coked Catalysts in a Polytropic Reactor. Ind Eng Chem Res 2005;44(14):5373–9. https://doi.org/10.1021/ie0491443.
[36] Wei Y, Li S, Jing J, Yang M, Jiang C, Chu W. Synthesis of Cu–Co Catalysts for Methanol Decomposition to Hydrogen Production via Deposition-Precipitation with Urea Method. Catal Letters 2019;149(10):2671–82. https://doi.org/10.1007/s10562-019-02731-9.
[37] Durán P, Esteban I, Francés E, Peña JA, Herguido J. Use of a fixed bed reactor with distributed feed to minimize thermal gradients for synthetic natural gas production. First Int. Conf. Unconv. Catal. React. Appl. UCRA2019, Zaragoza (Spain): TU Delft and Universidad Zaragoza; 2019.
[38] Durán P, Esteban I, Francés E, Herguido J, Peña JA. Methanation with Ni based catalyst using a fixed bed reactor with distributed feed. Influence of reactive feed allocation. HYCELTEC 2019, Barcelona (Spain): University of Barcelona; 2019, p. 76–8.